THE JOURNAL OF BIOLOGICAL CHEMISTRY VOL. 287, NO. 12, pp. 8912–8919, March 16, 2012

Unique Iron Coordination in Iron-chelating Molecule Vibriobactin Helps *Vibrio cholerae* Evade Mammalian Siderocalin-mediated Immune Response*[S]

Received for publication, October 20, 2011, and in revised form, January 24, 2012 Published, JBC Papers in Press, January 30, 2012, DOI 10.1074/jbc.M111.316034

Ning Li[‡], Conggang Zhang[‡], Bingqing Li[‡], Xiuhua Liu[‡§], Yan Huang[‡], Sujuan Xu[‡], and Lichuan Gu[‡1]

From the [‡]State Key Laboratory of Microbial Technology, Shandong University, Jinan 250100 and the [§]College of Life Sciences, Hebei University, Baoding 071002, China

Background: *Vibrio cholerae* uses vibriobactin to sequester iron. The structure of ferric vibriobactin is controversial.
Results: The three catechol moieties donate five, rather than six, oxygen atoms as iron ligands.
Conclusion: Ferric vibriobactin can evade the human immune protein siderocalin *in vitro* because of the special iron coordination.
Significance: The unique iron coordination could be used by pathogenic bacteria to evade the mammalian innate immune system of siderocalin.

Iron is essential for the survival of almost all bacteria. *Vibrio cholerae* acquires iron through the secretion of a catecholate siderophore called vibriobactin. At present, how vibriobactin chelates ferric ion remains controversial. In addition, the mechanisms underlying the recognition of ferric vibriobactin by the siderophore transport system and its delivery into the cytoplasm specifically have not been clarified. In this study, we report the high-resolution structures of the ferric vibriobactin periplasmic binding protein ViuP and its complex with ferric vibriobactin. The holo-ViuP structure reveals that ferric vibriobactin does not adopt the same iron coordination as that of other catecholate siderophores such as enterobactin. The three catechol moieties donate five, rather than six, oxygen atoms as iron ligands. The sixth iron ligand is provided by a nitrogen atom from the second oxazoline ring. This kind of iron coordination results in the protrusion of the second catechol moiety and renders the electrostatic surface potential of ferric vibriobactin less negatively polarized compared with ferric enterobactin. To accommodate ferric vibriobactin, ViuP has a deeper subpocket to hold the protrusion of the second catechol group. This structural characteristic has not been observed in other catecholate siderophore-binding proteins. Biochemical data show that siderocalin, which is part of the mammalian innate immune system, cannot efficiently sequester ferric vibriobactin *in vitro*, although it can capture many catecholate siderophores with high efficiency. Our findings suggest that the unique iron coordination found in ferric vibriobactin may be utilized by some pathogenic bacteria to evade the siderocalin-mediated innate immune response of mammals.

Iron is an essential ion for the growth of most bacteria. However, the concentration of soluble iron in the aqueous and aerobic environment is as low as 10^{-18} M, which is not sufficient for bacterial survival (1). Mammals have evolved a defensive mechanism against pathogenic bacteria by synthesizing iron-chelating proteins such as lactoferrin and transferrin, which push the free iron concentration to an extremely low level that does not support bacterial growth (2). To obtain sufficient iron, many bacteria have developed the ability to synthesize low-molecular weight, high-affinity iron chelators known as siderophores to scavenge iron with high efficiency (3). Siderophores can be divided into three groups: catecholates, hydroxamates (or α-hydroxymates), and carboxylates, among which catecholate siderophores are the most powerful iron chelators (4).

Vibrio cholerae, the causative agent of the severe diarrheal disease cholera (5), acquires iron through secretion of a catecholate siderophore called vibriobactin (6–8). Some strains of non-epidemic *V. cholerae* have the ability to cause wound infections and septicemia in susceptible people (9, 10). These strains need to obtain enough iron from the blood. Vibriobactin is synthesized from dihydroxybenzoyl, threonine, and norspermidine by a nonribosomal peptide synthesis-type system (8, 11–13). It is a catecholate-type siderophore like enterobactin. All catecholate siderophores contain three 2,3-dihydroxybenzoyl moieties. Studies have demonstrated that enterobactin uses six oxygens of 2,3-dihydroxybenzoic acid to coordinate ferric atom, leading to the formation of a $[Fe^{III}(Ent)]^{3-}$ complex[2] (14, 15). Thus far, the three-dimensional structure of vibriobactin has not been determined. Because vibriobactin contains three catechol moieties and two oxazolines (see Fig. 1*A*) (14, 16), the capacity of the nitrogen atom of the second oxazoline to coordinate the ferric atom is controversial (4, 6). The ferric atom bound in the siderophore is always in the high-spin d^5 electron configuration, so the crystal field energy is not large enough to stabilize the ferric siderophore complex. Most

* This work was supported by the State Key Laboratory of Microbial Technology of Shandong University and by Grant 2006AA02A324 from the Hi-Tech Research and Development Program of China.
[S] This article contains supplemental Figs. S1 and S2.
The atomic coordinates and structure factors (codes 3R5S and 3R5T) have been deposited in the Protein Data Bank, Research Collaboratory for Structural Bioinformatics, Rutgers University, New Brunswick, NJ (http://www.rcsb.org/).
[1] To whom correspondence should be addressed. Tel.: 86-531-8836-2039; E-mail: lcgu@sdu.edu.cn.

[2] The abbreviations used are: $[Fe^{III}(Ent)]^{3-}$, ferric enterobactin; PBP, periplasmic binding protein; SBP, siderophore-binding protein; $[Fe^{III}(Vib)]^{2-}$, ferric vibriobactin.

of the stable energy comes from Lewis acid-base electronic energy because the ferric atom is a strong Lewis acid, and oxygen atoms are hard Lewis bases (1, 4). Because nitrogen is a softer atom compared with oxygen, we can assume that the capacity of nitrogen to coordinate with ferric atom is weaker than that of oxygen. Definitive evidence has not been obtained to clarify whether the nitrogen atom of the second oxazoline coordinates the ferric atom or not.

The secreted vibriobactin forms a ferric vibriobactin complex when an iron is chelated. The ferric vibriobactin complex is then transported to the cytoplasm of *V. cholerae* by a series of transport proteins, including ViuAPDGC, in which ViuA is an outer membrane receptor for vibriobactin and ViuPDGC forms a periplasmic binding protein-dependent ATP-binding cassette transport system (7, 18). The mechanism by which vibriobactin is recognized and delivered into the periplasmic space by Gram-negative bacteria is unknown. In *V. cholerae*, ViuP has the ability to transport ferric vibriobactin from the outer membrane to the inner membrane. As a periplasmic receptor of ferric vibriobactin, ViuP needs to distinguish ferric vibriobactin from free vibriobactin. Furthermore, holo-ViuP needs to be recognized by the ATP-binding cassette transporter ViuDGC and release ferric vibriobactin in the process of siderophore transportation.

In this study, we present high-resolution structures of the vibriobactin periplasmic binding protein ViuP and its complex with ferric vibriobactin. The structure of holo-ViuP shows that ferric vibriobactin does not adopt the same iron coordination as that of other catecholate siderophores such as enterobactin. Significantly, although the structure of ViuP shows that it is a type III periplasmic binding protein (PBP), we found that the position of the ferric vibriobactin-binding pocket is located at the opposite site of the protein compared with all other siderophore-binding type III PBPs.

EXPERIMENTAL PROCEDURES

Protein Expression and Purification—The open reading frame of ViuP (residues 27–325) was amplified from the genome of *V. cholerae* O1 bv. El Tor strain N16961. Residues 1–26 were truncated because they were predicted to be a signal peptide by the SignalP 3.0 server. The gene was then subcloned into the pET21b vector (Novagen) between the NdeI and XhoI restriction sites. The plasmid was transferred into *Escherichia coli* BL21(DE3) cells. The transformed BL21(DE3) cells were cultured in 6 liters of LB medium supplemented with 100 μg/ml ampicillin at 37 °C to $A_{600} = 0.8$. The medium was cooled to 22 °C, and protein expression was induced by the addition of isopropyl β-D-thiogalactopyranoside to a final concentration of 0.18 mM. Cells were harvested by centrifugation after 12 h of expression. The pellet was resuspended in lysis buffer (25 mM Tris-HCl (pH 8.0) and 200 mM NaCl) and lysed by sonication. The cell lysate was then centrifuged for 45 min at 28,500 $\times$ *g*. Soluble fractions were loaded onto a nickel-chelating Sepharose affinity column (GE Healthcare) equilibrated with lysis buffer. The elution product was further purified by anion exchange chromatography and gel filtration chromatography. The purified protein was stored at −80 °C until used. Selenomethionyl-substituted ViuP was overexpressed in the BL21(DE3) cells using M9 medium. During incubation, selenomethionine was added to the medium, and cells were induced with isopropyl β-D-thiogalactopyranoside. The selenomethionyl-substituted ViuP was purified with the same protocol used for native ViuP.

Crystallization and Data Collection—Native ViuP was screened for crystals with a Hampton Research crystal screen kit using the hanging drop method. ViuP crystals appropriate for data collection appeared under conditions of 0.2 M ammonium acetate, 0.1 M sodium acetate (pH 4.6), and 25% polyethylene glycol 4000. Selenomethionyl-substituted ViuP crystals were also obtained under the same conditions. To obtain crystals of holo-ViuP, ferric vibriobactin (EMC Co.) was dissolved in Me_2SO to a concentration of 20 mM. The resulting solution was added to native ViuP until the ligand/protein molar ratio was 3:1. Holo-ViuP crystals were grown at 18 °C using the hanging drop method as described for native ViuP. The best holo-ViuP crystals were obtained under the same conditions as used for native ViuP. For cryo-crystallography experiments, all crystals were soaked in a solvent identical to the reservoir solution with a final concentration of 20% glycerol. All data sets were collected at Shanghai Synchrotron Radiation facility beamline BL17U1 and were processed with HKL2000 software (19). Crystals of apo-ViuP belong to space group C2 with unit cell dimensions $a = 76.925$, $b = 61.068$, and $c = 66.852$ Å, whereas crystals of holo-ViuP belong to space group C2 with unit cell dimensions $a = 82.496$, $b = 55.545$, and $c = 69.542$ Å. Detailed statistical data are presented in Table 1.

Phasing and Model Refinement—The structure of apo-ViuP was solved with the single-wavelength anomalous diffraction phasing method. Four selenium sites were found using the SOLVE program. RESOLVE (20–22) was used to improve the initial single-wavelength anomalous diffraction phases and to automatically trace the chain of ViuP. The initial model was built with the COOT program and refined with PHENIX suite software (23). Five percent of the reflection data were set aside for calculation of the free *R*-factor throughout the refinement progress. The three-dimensional structure of holo-ViuP was solved with the molecule replacement method using apo-ViuP as the search model. The same protocol was followed for model building and refinement of the holo-ViuP structure. Refinement of holo-ViuP produced a reliable structure at a resolution of 1.45 Å, with >90% of the residues located in the most favored of Ramachandran plot region. The existence and structure of the ferric vibriobactin complex were determined according to the $2F_o - F_c$ and $F_o - F_c$ electron density maps.

Fluorescence Quenching Analysis—The recombinant siderocalin gene was subcloned from the human genome cDNA. The siderocalin protein was purified from an *entF* knock-out BL21(DE3) strain and purified following the same protocols used for ViuP. Fluorescence quenching of recombinant siderocalin was measured on a Hitachi F-4500 fluorescence spectrophotometer with a 2.5-nm slit band pass and the characteristic excitation and emission wavelengths of 281 and 340 nm, respectively. Prior to the experiment, the siderocalin solution was diluted to a concentration of 200 nM in Tris-HCl buffer solution (pH 7.4) containing 5% Me_2SO. The ferric vibriobactin solution was diluted with Tris-HCl buffer solution containing

TABLE 1
Statistics of crystallographic analysis

	Apo-ViuP	Holo-ViuP
Data collection		
Space group	C2	C2
Cell dimensions	$a = 76.93$, $b = 61.07$, $c = 66.85$ Å; $\alpha = 90.00°$, $\beta = 120.56°$, $\gamma = 90.00°$	$a = 82.50$, $b = 55.55$, $c = 69.54$ Å; $\alpha = 90.00°$, $\beta = 117.02°$, $\gamma = 90.00°$
Resolution (Å)	50-1.79 (1.85-1.79)[a]	50-1.45 (1.50-1.45)
Completeness (%)	98.7 (88.2)	97.6 (88.0)
Redundancy	3.7 (3.3)	3.5 (2.5)
$I/\sigma(I)$	27.56 (3.98)	18 (3.16)
R_{sym} (%)[b]	5.0 (25.1)	6.0 (31.5)
Refinement		
Resolution	33.12-1.79	24.6-1.45
R_{work}/R_{free} (%)	0.177/0.213	0.182/0.209
r.m.s.d.[c]		
Bond lengths (Å)	0.007	0.007
Bond angles	1.0°	1.2°
Ramachandran plot (%)[d]		
Most favored (%)	94.1	92.1
Additionally allowed (%)	5.9	7.9
Generously allowed (%)	0	0
Disallowed (%)	0	0

[a] Values in parentheses are for reflections in the highest resolution shell.
[b] $R_{sym} = \sum_{hkl}\sum_i|I(hkl)_i - \langle I(hkl)\rangle|/\sum_{hkl}\sum I\langle I(hkl)_i\rangle$ over i observations.
[c] r.m.s.d., root mean square deviation.
[d] As defined in PROCHECK.

FIGURE 1. **Schematic representation of vibriobactin, overall structure of ViuP, and superposition of apo-ViuP and holo-ViuP.** *A*, chemical structure of vibriobactin. The three catechol groups are indicated by *A*, *B*, and *C*. *B*, illustration of the structure shows the two domains of ViuP connected by an α-helix. The surface is in *light orange*. *C*, least-squares alignment of apo-ViuP (*gray*) and holo-ViuP with ferric vibriobactin (*red*). The Cα backbone is shown as a ribbon model.

5% Me_2SO to a concentration of 20 μM. Ferric enterobactin and vibriobactin were also diluted to a concentration of 20 μM with Tris-HCl buffer solution containing 5% Me_2SO. All fluorescence values were corrected for dilution with the addition of the ligand. Fluorescence data were analyzed with DYNAFIT (24) by nonlinear regression analysis of the fluorescence response to ligand concentration with the one-site binding model. Dissociation constants (K_d) for ligands bound to siderocalin were determined using the DYNAFIT results.

RESULTS AND DISCUSSION

Overall Structure of ViuP—ViuP is a periplasmic transport protein that transports ferric vibriobactin from the outer membrane to the inner membrane of *V. cholerae*. Crystals of apo-ViuP and ferric vibriobactin bound to ViuP diffracted to resolutions of 1.79 and 1.45 Å, respectively. The structure of apo-ViuP was solved with the selenium single-wavelength anomalous diffraction method, after which the structure of holo-ViuP was solved using the molecular replacement method with the apo-ViuP structure as the search model. Data collection, phasing, and refinement statistics are detailed in Table 1. ViuP has a typical bilobal shape, with the two independent domains linked by a 21-residue α-helix (residues 165–185). The five-stranded β-sheet of the N-terminal domain and the six-stranded β-sheet of the C-terminal are sandwiched by several α-helices, forming a Rossmann-like fold (Fig. 1*B*). Similar structural features have been observed in other siderophore-binding proteins (SBPs) such as CeuE, FeuA, and YclQ (25–27). The structure of holo-ViuP shows that ferric vibriobactin is located in a shallow pocket in the middle part of the bilobal structure formed by the two domains. Compared with the structure of apo-ViuP, the two domains are more closely related in holo-ViuP to accommodate the substrate after binding of ferric vibriobactin (Fig. 1*C*).

Ferric Vibriobactin-binding Site—The ferric vibriobactin-binding site of ViuP is composed of 10 residues (Val-59, Thr-60, Thr-78, Thr-79, Gln-80, Phe-84, Gly-124, Ala-125, Asp-126, and Tyr-146) from the N-terminal domain and nine residues (Ser-197, His-199, Ala-206, His-239, Asp-241, Phe-242, Arg-244, Phe-296, and Arg-297) from the C-terminal domain (Fig. 2*B*). Three subpockets are formed to accommodate the three catecholate groups of vibriobactin (Fig. 2*C*). The subpocket that holds the protruding catechol moiety is visibly deeper than the two other subpockets, so the local protrusion can fit. Ferric vibriobactin is stabilized mainly by the hybrid electrostatic/cation-π interactions with Arg-244 and Arg-297 (Fig. 2*A*) and the

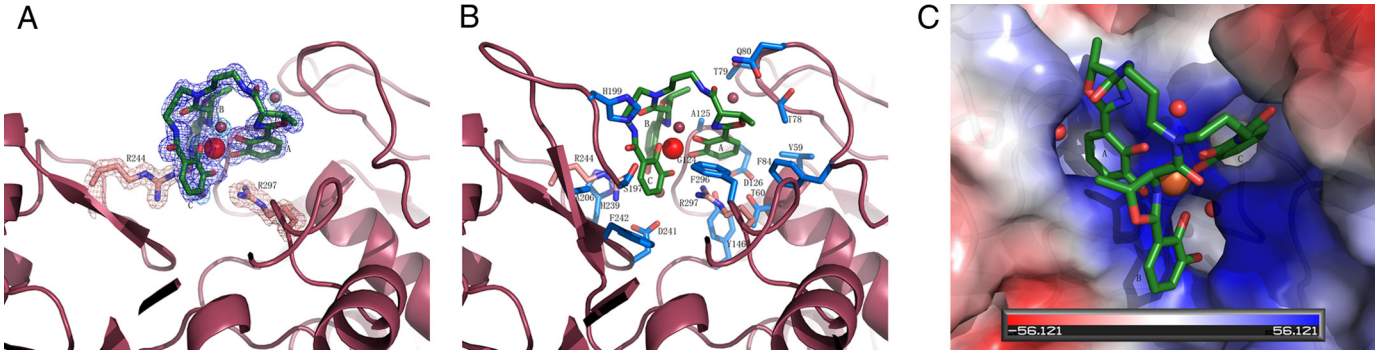

FIGURE 2. **Detailed view of vibriobactin pocket of ViuP.** Ligand atoms are shown in *green* (carbon), *red* (oxygen), *blue* (nitrogen), and as a *red sphere* (iron). *A*, $2F_o - F_c$ electron density map calculated at 1.45 Å resolution (contour level of 1.5) for ferric vibriobactin and the three water molecules (*salmon*). The electron density map shows that Arg-244 and Arg-297 form hydrogen bonds with vibriobactin. *B*, illustration of the side chains of other residues that compose the binding pocket. Carbons are in *light blue*. *C*, electrostatic surface model of the binding pocket.

hydrophobic interactions with Thr-78, Thr-79, Phe-84, Ile-123, Gly-124, Ala-125, Ala-206, Phe-242, and Phe-296. Superposition of the apo- and holo-ViuP structures using a least-squares algorithm with the C-terminal domain revealed that the side chains of the Arg-244 and Arg-297 basic diad are reoriented to form interactions with ferric vibriobactin. The norspermidine backbone is not involved in interactions with the protein. Three water molecules (*e.g.* positions 3, 6, and 90) fill the vacant space between ferric vibriobactin and the binding site (Fig. 2*A*). These typical protein-siderophore interactions have been observed in all crystal structures of a PBP in complex with catecholate siderophores (25–27).

The structure of ViuP clearly indicates that it is a type III PBP. Unexpectedly, even though the overall structures of type III PBPs are conserved, multiple-sequence alignment of ViuP with other type III siderophore-binding PBPs revealed sequence identities below 20% (Fig. 3). CeuE, FeuA, and YclQ are catecholate SBPs and are type III PBPs with two domains linked by a long α-helix. Structural comparisons of these three proteins with ViuP using the Dali server yielded a root mean square deviation of 3 Å for ~240 Cα atoms. The catecholate siderophores transported by these three SBPs all use six oxygens to coordinate with iron and use a basic triad to balance the three negative charges of the ferric siderophore. In contrast, a basic dyad was found in the active site of ViuP. This finding suggests that ferric vibriobactin may have two, rather than three, negative charges. Although the Arg-244 and Arg-297 basic dyad that stabilizes ferric vibriobactin is not conserved, Glu-108 and Glu-248 of ViuP are highly conserved residues that may specifically interact with ViuDG to deliver ferric vibriobactin.

The low sequence identity to other SBPs indicates that ViuP may belong to a new subgroup of type III PBPs. Comparison of the structure of ViuP with other type III siderophore-binding PBPs revealed that the binding pocket of ferric vibriobactin is located at the opposite side of the protein (Fig. 4). This finding suggests that ViuP and other known catecholate siderophore-binding PBPs may have evolved to the same fold via convergent evolution from different ancestral proteins. At the same time, ViuP contains two conserved Glu residues (Glu-108 and Glu-248) at the same positions as other SBPs, so the mechanism of ferric vibriobactin transfer should be similar to that of other SBPs.

Special Iron Coordination—Vibriobactin is a catecholate siderophore with two oxazole rings. The exact mechanism for iron coordination of ferric vibriobactin is controversial. Griffiths *et al.* (6) suggested that the nitrogen atom of the second oxazole may participate in iron coordination, whereas Miethke *et al.* (4) proposed that the six oxygen atoms from the three catechol moieties coordinate with the ferric atom. The high-resolution structure of holo-ViuP found in this study supports the former hypothesis. The three catechol moieties donate five, rather than six, oxygen atoms as iron ligands. The sixth iron ligand is provided by a nitrogen atom from the second oxazoline ring (Fig. 5 and supplemental Fig. S1*B*). This iron coordination is unusual because all other catecholate siderophores studied so far achieve iron coordination using six oxygen atoms from the three catechol moieties. The structure of ferric vibriobactin is reliable because the diffraction data have a high resolution of 1.45 Å, and the electron density of ferric vibriobactin is crystal clear. This type of coordination gives ferric vibriobactin unique structural and chemical features in comparison with other iron-laden catecholate siderophores such as enterobactin. First, a protrusion of the second catechol moiety (Moiety B) was formed due to the outward movement of the ligand oxygen atom. To specifically recognize ferric vibriobactin, the subpocket holding the second catechol moiety is deeper than the other two subpockets in ViuP. Second, ferric vibriobactin carries two, rather than three, negative charges, which are typical of the common iron-laden catecholate siderophores that use six oxygen atoms from the catechol moieties as iron ligands. The less negative charge of the ferric vibriobactin ($[Fe^{III}(Vib)]^{2-}$) in contrast to other iron-laden triscatecholate siderophores is compatible with the basic dyad structure of ViuP. In contrast, the basic triad is a widespread binding motif for triscatecholate siderophores in all structures reported previously (25–27).

Ferric Vibriobactin Binds to Siderocalin with Low Affinity—Previous studies showed that the mammalian innate immune system protein siderocalin sequesters iron-laden catecholate siderophores with high affinity through specific hybrid electrostatic/cation-π interactions with the iron-coordinated catechol moieties (30–32). Vibriobactin contains three catechol moieties that can be expected to adopt the same iron coordination as other catecholate siderophores, so $[Fe^{III}(Vib)]^{2-}$ can be reasonably expected to also be bound by siderocalin (33). However,

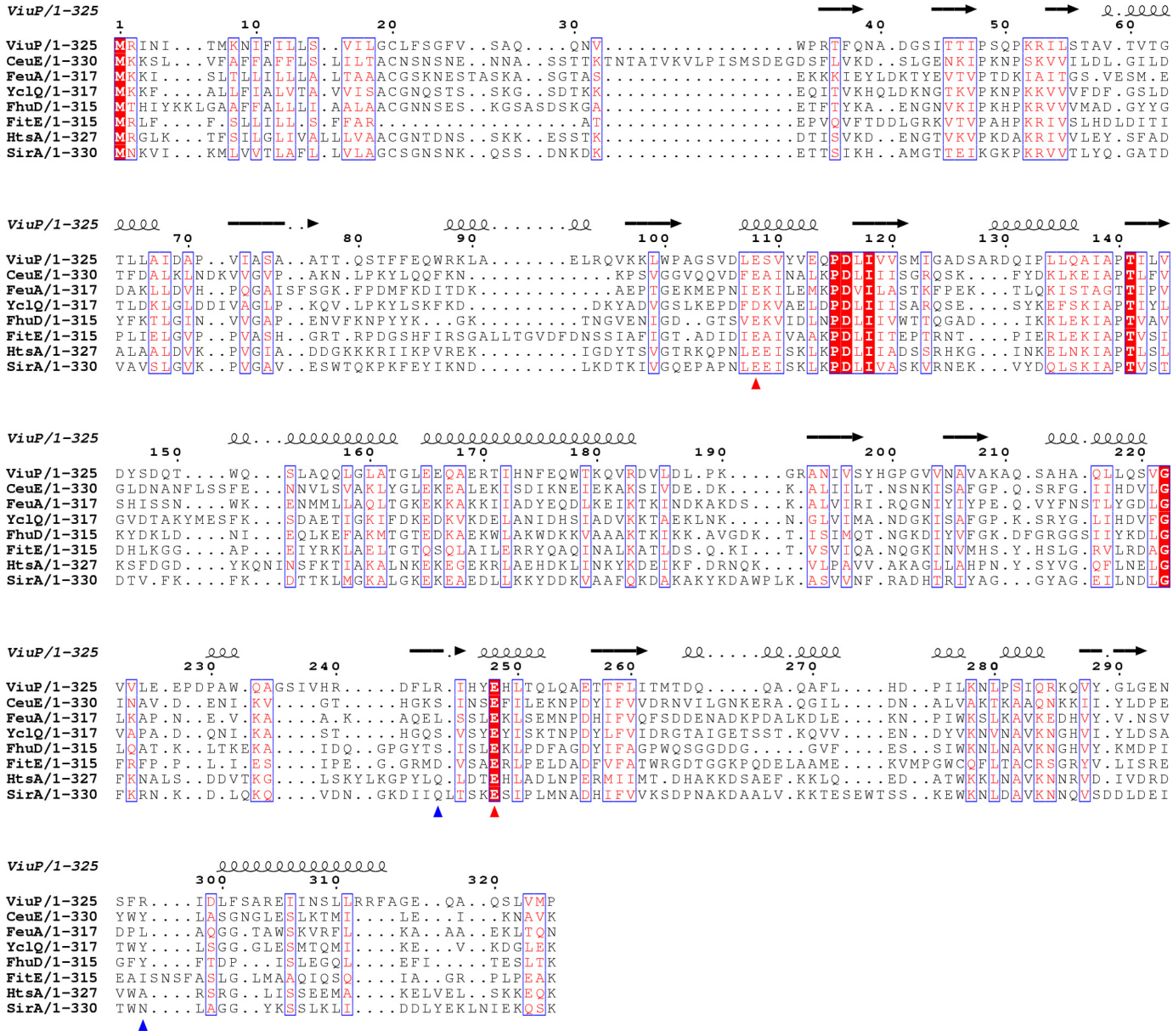

FIGURE 3. **Sequence alignment of known SBPs.** The sequences of ViuP from *V. cholerae* (Protein Data Bank code 3R5S), CeuE from *Campylobacter jejuni* (PDB code 2CHU), FeuA from *Bacillus subtilis* (code 2PHZ), YclQ from *B. subtilis* (code 3GFV), FhuD from *E. coli* (code 1EFD), FitE from *E. coli* (code 3BE6), HtsA from *Staphylococcus aureus* (code 3EIW), and SirA from *S. aureus* (code 3MWG) were aligned using T-Coffee (28) and prepared using the online program ESPript (29). The secondary structure is represented by α-helix and β-sheet. *Blue arrowheads* indicate the positions of the basic dyad of ViuP. *Red arrowheads* indicate the positions of Glu residues of ViuP that may interact with the corresponding ATP-binding cassette transporter ViuDGC.

the unique iron coordination observed in our study raises the question of whether $[Fe^{III}(Vib)]^{2-}$ can escape from capture by siderocalin. To investigate the possible interactions between $[Fe^{III}(Vib)]^{2-}$ and siderocalin, $[Fe^{III}(Vib)]^{2-}$ was overlaid on the structure of $[Fe^{III}(Ent)]^{3-}$ bound to siderocalin (Fig. 5*B*). We observed a severe steric clash between the protruding catechol moiety and the corresponding subpocket due to the unusual stereochemistry of the iron coordination. Thus, we speculate that the interactions between $[Fe^{III}(Vib)]^{2-}$ and siderocalin would be much weaker than those between $[Fe^{III}(Ent)]^{3-}$ and siderocalin. To test this hypothesis, we evaluated the interactions between siderocalin and $[Fe^{III}(Vib)]^{2-}$ and between iron-free vibriobactin and $[Fe^{III}(Ent)]^{3-}$ by the fluorescence quenching analysis method (Fig. 6).

The results indicate that siderocalin binds $[Fe^{III}(Ent)]^{3-}$ with high affinity with a K_d as low as 2.65 ± 0.63 nM. In the case of iron-free vibriobactin, the K_d is ~197.50 ± 6.33 nM. This finding suggests that iron-free vibriobactin binds to siderocalin much more weakly than $[Fe^{III}(Ent)]^{3-}$. This result is not surprising because iron coordination is necessary for the right stereochemistry and the negative charges of the catecholate siderophore. Previous data showed that the binding affinity of iron-free enterobactin for siderocalin is much weaker than that of ferric enterobactin (32). However, in the present study, $[Fe^{III}(Vib)]^{2-}$ bound to siderocalin with a much lower binding affinity compared with iron-free vibriobactin. The dissociation constant of $[Fe^{III}(Vib)]^{2-}$ is 1419.60 ± 48.92 nM, which is ~700-fold greater than that of $[Fe^{III}(Ent)]^{3-}$. This finding

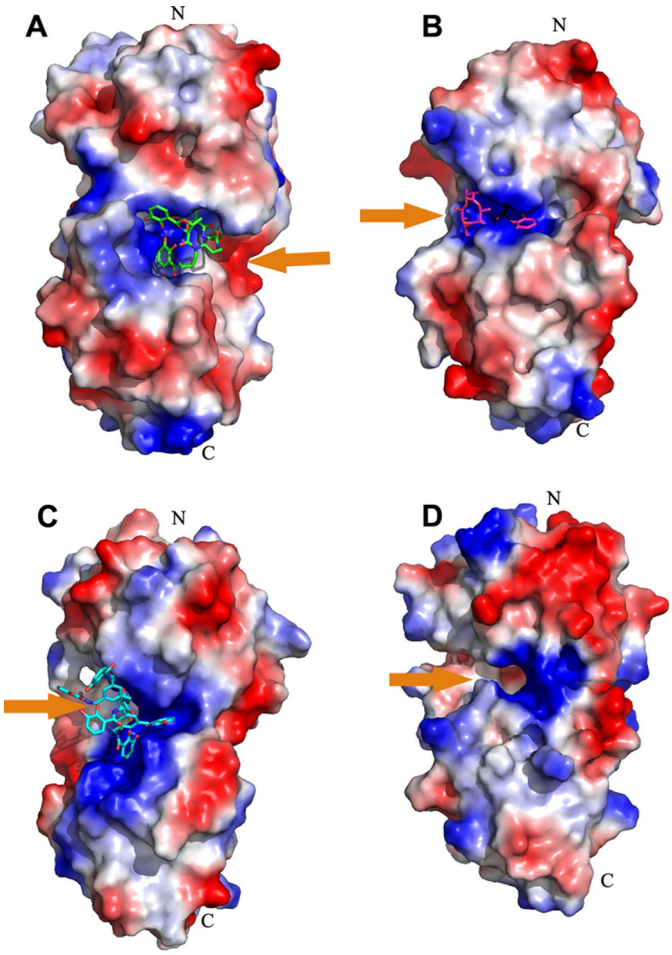

FIGURE 4. **Electrostatic potential map of binding pocket of known catecholate siderophore-binding PBPs.** All catecholate siderophore-binding PBPs were displayed with the same orientation of the N- and C-terminal domains. *Orange arrows* represent the orientation of the binding pocket for ferric vibriobactin. *A*, ViuP; *B*, FeuA (Protein Data Bank code 2WHY); *C*, CeuE (code 2CHU); *D*, YclQ (code 3GFV) (25–27). The pocket of vibriobactin is on the right side of ViuP, whereas all of the other pockets are on the left side of associated PBPs.

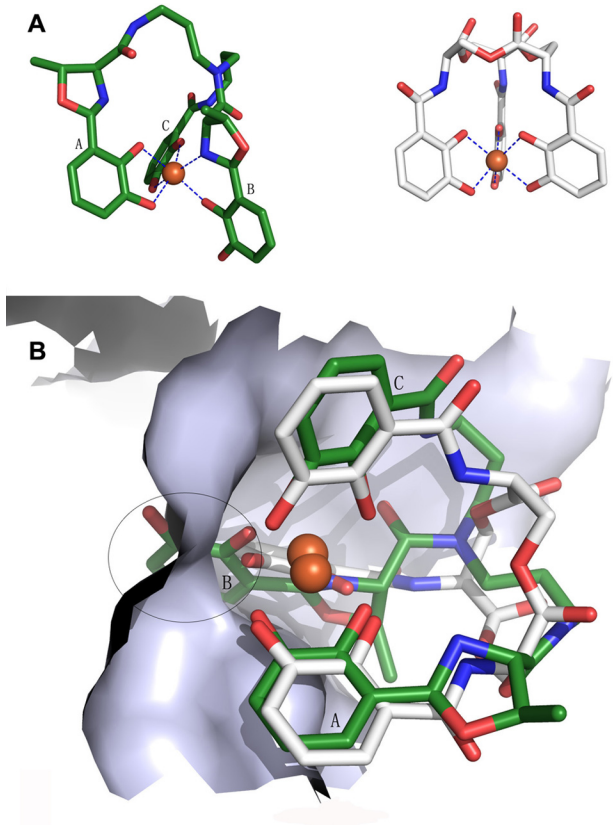

FIGURE 5. **Ferric atom coordination of enterobactin and vibriobactin and superimposed result of $[Fe^{III}(Vib)]^{2-}$ and $[Fe^{III}(Ent)]^{3-}$.** *A*, *blue dashed lines* represent the coordination bond. Ferric vibriobactin is on the left, and ferric enterobactin is on the right. $[Fe^{III}(Ent)]^{3-}$ has a 3-fold symmetry axis. *B*, the *white* skeleton stick structure is enterobactin, and the *green* structures are vibriobactin superimposed on enterobactin at the binding site. The *encircled* region indicates the conflict between $[Fe^{III}(Vib)]^{2-}$ and siderocalin when siderocalin chelates $[Fe^{III}(Vib)]^{2-}$ at the calyx that binds $[Fe^{III}(Ent)]^{3-}$.

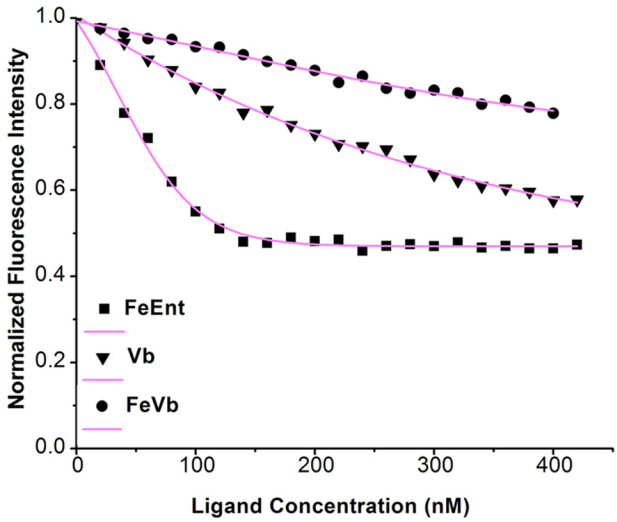

FIGURE 6. **Fluorescence quenching analyses of capacity of siderocalin to bind ferric enterobactin (*FeEnt*), vibriobactin (*Vb*), and ferric vibriobactin (*FeVb*).** Fluorescence data were taken at 340 nm (pH 7.4) upon the addition of substrates to a 200 nM solution of siderocalin. *Data points* indicate the fluorescence signals generated by siderocalin, and *curves* indicate the calculated fits.

strongly suggests that iron-laden vibriobactin is not favorable for binding by siderocalin. Consequently, the innate immune protein siderocalin is not as effective against $[Fe^{III}(Vib)]^{2-}$ as against $[Fe^{III}(Ent)]^{3-}$ *in vitro*. This means that *V. cholerae* may evade human siderocalin to acquire sufficient iron, although more *in vivo* data are needed to support this argument.

Structural analysis of $[Fe^{III}(Vib)]^{2-}$ and siderocalin revealed that three factors contribute to the successful escape of $[Fe^{III}(Vib)]^{2-}$. First, the unique iron coordination results in the protrusion of one catechol moiety. The potential steric clash makes the three catechol moieties of $[Fe^{III}(Vib)]^{2-}$ and the three subpockets of siderocalin incompatible with each other. Second, $[Fe^{III}(Vib)]^{2-}$ has two, rather than three, negative charges due to the substitution of the nitrogen atom as a ligand. The less net negative charge results in weaker hybrid electrostatic/cation-π interactions with the highly positively charged active site of siderocalin. Third, in contrast to $[Fe^{III}(Ent)]^{3-}$, $[Fe^{III}(Vib)]^{2-}$ is not a symmetric molecule and does not have a rotational axis (Fig. 5*A*). Upon binding to ferric iron, the scaffold of $[Fe^{III}(Vib)]^{2-}$ adopts an extremely distorted conformation that is not conducive to sequestration by siderocalin (Fig. 5*B*).

Previous studies have shown that the ability to evade siderocalin of the innate immune system is necessary for many pathogenic bacteria to achieve successful infection (30, 34, 35). Thus far, two strategies have been observed in pathogenic bacteria. Many pathogenic enteric bacteria, including *E. coli*, *Salmonella* spp., and *Klebsiella pneumonia*, have an *iroA* gene cluster that encodes enzymes that produce glycosylated derivatives of enterobactin. *Bacillus anthracis* evades siderocalin through production of a stealth siderophore, which has a 3,4-dihydroxybenzoyl iron-chelating subunit rather than the common 2,3-dihydroxybenzoyl. In this study, the unique iron coordination of $[Fe^{III}(Vib)]^{2-}$ allows it to escape sequestration by siderocalin *in vitro*. This finding suggests that ferric vibriobactin may function as a stealth siderophore for *V. cholerae*. Previous studies have shown that vibriobactin is an important virulence factor and that strains with mutations in vibriobactin biosynthesis have decreased virulence in mice (36). Although no *in vivo* data on whether the ability of *V. cholerae* to evade siderocalin is necessary for successful infection are available, the present study presents a feasible mechanism for a catecholate siderophore to escape siderocalin. This mechanism could be important for the non-epidemic *V. cholerae* that faces higher concentrations of siderocalin in blood while causing wounds, ear infections, or septicemia (9, 10). *Vibrio vulnificus*, which can cause lethal septicemia and wound infection in humans, produces vulnibactin, a siderophore with a structure similar to that of vibriobactin (37). Therefore, we can reasonably expect that *V. vulnificus* may employ a similar mechanism to evade siderocalin (supplemental Fig. S2). In addition, *V. cholerae* is not the only bacterium that utilizes vibriobactin (17), so we can speculate that some pathogenic bacteria may use this mechanism to evade the siderocalin-mediated mammalian innate immune response.

Acknowledgments—The genomic DNA of V. cholerae was a gift from Prof. Bonnie Bassler. We acknowledge Prof. Chengjiang Gao for providing the human cDNA library. We thank Prof. Yulong Shen and Pengjuan Liang for assistance in gene cloning, Prof. Nieng Yan for critical reading of this manuscript, Dr. Roberta Greenwood (Shandong University) for linguistic advice, and Dr. Zhiwei Huang and the staff of beamline BL17U1 at the Shanghai Synchrotron Radiation Facility for support with data collection.

REFERENCES

1. Raymond, K. N., and Carrano, C. J. (1979) Coordination chemistry and microbial iron transport. *Acc. Chem. Res.* **12,** 183–190
2. Arnold, R. R., Cole, M. F., and McGhee, J. R. (1977) A bactericidal effect for human lactoferrin. *Science* **197,** 263–265
3. Braun, V., Hantke, K., and Köster, W. (1998) Bacterial iron transport: mechanisms, genetics, and regulation. *Met. Ions Biol. Syst.* **35,** 67–145
4. Miethke, M., and Marahiel, M. A. (2007) Siderophore-based iron acquisition and pathogen control. *Microbiol. Mol. Biol. Rev.* **71,** 413–451
5. Faruque, S. M., Albert, M. J., and Mekalanos, J. J. (1998) Epidemiology, genetics, and ecology of toxigenic *Vibrio cholerae*. *Microbiol. Mol. Biol. Rev.* **62,** 1301–1314
6. Griffiths, G. L., Sigel, S. P., Payne, S. M., and Neilands, J. B. (1984) Vibriobactin, a siderophore from *Vibrio cholerae*. *J. Biol. Chem.* **259,** 383–385
7. Butterton, J. R., Stoebner, J. A., Payne, S. M., and Calderwood, S. B. (1992) Cloning, sequencing, and transcriptional regulation of *viuA*, the gene encoding the ferric vibriobactin receptor of *Vibrio cholerae*. *J. Bacteriol.* **174,** 3729–3738
8. Wyckoff, E. E., Stoebner, J. A., Reed, K. E., and Payne, S. M. (1997) Cloning of a *Vibrio cholerae* vibriobactin gene cluster: identification of genes required for early steps in siderophore biosynthesis. *J. Bacteriol.* **179,** 7055–7062
9. Mulder, G. D., Ries, T. M., and Beaver, T. R. (1989) Nontoxigenic *Vibrio cholerae* wound infection after exposure to contaminated lake water. *J. Infect. Dis.* **159,** 809–811
10. Morris, J. G., Jr. (2003) Cholera and other types of vibriosis: a story of human pandemics and oysters on the half shell. *Clin. Infect. Dis.* **37,** 272–280
11. Butterton, J. R., and Calderwood, S. B. (1994) Identification, cloning, and sequencing of a gene required for ferric vibriobactin utilization by *Vibrio cholerae*. *J. Bacteriol.* **176,** 5631–5638
12. Butterton, J. R., Choi, M. H., Watnick, P. I., Carroll, P. A., and Calderwood, S. B. (2000) *Vibrio cholerae* VibF is required for vibriobactin synthesis and is a member of the family of nonribosomal peptide synthetases. *J. Bacteriol.* **182,** 1731–1738
13. Wyckoff, E. E., Smith, S. L., and Payne, S. M. (2001) VibD and VibH are required for late steps in vibriobactin biosynthesis in *Vibrio cholerae*. *J. Bacteriol.* **183,** 1830–1834
14. Raymond, K. N., Dertz, E. A., and Kim, S. S. (2003) Enterobactin: an archetype for microbial iron transport. *Proc. Natl. Acad. Sci. U.S.A.* **100,** 3584–3588
15. Karpishin, T. B., and Raymond, K. N. (1992) The first structural characterization of a metal-enterobactin complex: $[V(enterobactin)]^{2-}$. *Angew. Chem. Int. Ed. Engl.* **31,** 466–468
16. Dertz, E. A., Xu, J., Stintzi, A., and Raymond, K. N. (2006) Bacillibactin-mediated iron transport in *Bacillus subtilis*. *J. Am. Chem. Soc.* **128,** 22–23
17. Bergeron, R. J., and Weimar, W. R. (1990) Kinetics of iron acquisition from ferric siderophores by *Paracoccus denitrificans*. *J. Bacteriol.* **172,** 2650–2657
18. Wyckoff, E. E., Valle, A. M., Smith, S. L., and Payne, S. M. (1999) A multifunctional ATP-binding cassette transporter system from *Vibrio cholerae* transports vibriobactin and enterobactin. *J. Bacteriol.* **181,** 7588–7596
19. Otwinowski, Z., and Minor, W. (1997) Processing of x-ray diffraction data collected in oscillation mode. *Methods Enzymol.* **276,** 307–326
20. Terwilliger, T. C., and Berendzen, J. (1999) Automated MAD and MIR structure solution. *Acta Crystallogr. D Biol. Crystallogr.* **55,** 849–861
21. Terwilliger, T. C. (2000) Maximum-likelihood density modification. *Acta Crystallogr. D Biol. Crystallogr.* **56,** 965–972
22. Terwilliger, T. C. (2003) Automated main-chain model building by template matching and iterative fragment extension. *Acta Crystallogr. D Biol. Crystallogr.* **59,** 38–44
23. Adams, P. D., Afonine, P. V., Bunkóczi, G., Chen, V. B., Davis, I. W., Echols, N., Headd, J. J., Hung, L. W., Kapral, G. J., Grosse-Kunstleve, R. W., McCoy, A. J., Moriarty, N. W., Oeffner, R., Read, R. J., Richardson, D. C., Richardson, J. S., Terwilliger, T. C., and Zwart, P. H. (2010) *PHENIX*: a comprehensive Python-based system for macromolecular structure solution. *Acta Crystallogr. D Biol. Crystallogr.* **66,** 213–221
24. Kuzmic, P. (1996) Program DYNAFIT for the analysis of enzyme kinetic data: application to HIV proteinase. *Anal. Biochem.* **237,** 260–273
25. Müller, A., Wilkinson, A. J., Wilson, K. S., and Duhme-Klair, A. K. (2006) An $[\{Fe(mecam)\}_2]^{6-}$ bridge in the crystal structure of a ferric enterobactin-binding protein. *Angew. Chem. Int. Ed. Engl.* **45,** 5132–5136
26. Peuckert, F., Miethke, M., Albrecht, A. G., Essen, L. O., and Marahiel, M. A. (2009) Structural basis and stereochemistry of triscatecholate siderophore binding by FeuA. *Angew. Chem. Int. Ed. Engl.* **48,** 7924–7927
27. Zawadzka, A. M., Kim, Y., Maltseva, N., Nichiporuk, R., Fan, Y., Joachimiak, A., and Raymond, K. N. (2009) Characterization of a *Bacillus subtilis* transporter for petrobactin, an anthrax stealth siderophore. *Proc. Natl. Acad. Sci. U.S.A.* **106,** 21854–21859
28. Notredame, C., Higgins, D. G., and Heringa, J. (2000) T-Coffee: a novel method for fast and accurate multiple-sequence alignment. *J. Mol. Biol.* **302,** 205–217
29. Gouet, P., Courcelle, E., Stuart, D. I., and Métoz, F. (1999) ESPript: analysis of multiple-sequence alignments in PostScript. *Bioinformatics* **15,** 305–308

30. Flo, T. H., Smith, K. D., Sato, S., Rodriguez, D. J., Holmes, M. A., Strong, R. K., Akira, S., and Aderem, A. (2004) Lipocalin 2 mediates an innate immune response to bacterial infection by sequestrating iron. *Nature* **432,** 917–921
31. Holmes, M. A., Paulsene, W., Jide, X., Ratledge, C., and Strong, R. K. (2005) Siderocalin (Lcn2) also binds carboxymycobactins, potentially defending against mycobacterial infections through iron sequestration. *Structure* **13,** 29–41
32. Abergel, R. J., Clifton, M. C., Pizarro, J. C., Warner, J. A., Shuh, D. K., Strong, R. K., and Raymond, K. N. (2008) The siderocalin/enterobactin interaction: a link between mammalian immunity and bacterial iron transport. *J. Am. Chem. Soc.* **130,** 11524–11534
33. Strong, R. K. (2005) in Lipocalins (Åkerstrom, B., Borregaard, N., Flower, D. R., and Salier, J.-P., eds) pp. 83–98, Landes Bioscience, Austin, TX
34. Abergel, R. J., Wilson, M. K., Arceneaux, J. E., Hoette, T. M., Strong, R. K., Byers, B. R., and Raymond, K. N. (2006) Anthrax pathogen evades the mammalian immune system through stealth siderophore production. *Proc. Natl. Acad. Sci. U.S.A.* **103,** 18499–18503
35. Fischbach, M. A., Lin, H., Zhou, L., Yu, Y., Abergel, R. J., Liu, D. R., Raymond, K. N., Wanner, B. L., Strong, R. K., Walsh, C. T., Aderem, A., and Smith, K. D. (2006) The pathogen-associated *iroA* gene cluster mediates bacterial evasion of lipocalin 2. *Proc. Natl. Acad. Sci. U.S.A.* **103,** 16502–16507
36. Henderson, D. P., and Payne, S. M. (1994) *Vibrio cholerae* iron transport systems: roles of heme and siderophore iron transport in virulence and identification of a gene associated with multiple iron transport systems. *Infect. Immun.* **62,** 5120–5125
37. Okujo, N., Saito, M., Yamamoto, S., Yoshida, T., Miyoshi, S., and Shinoda, S. (1994) Structure of vulnibactin, a new polyamine-containing siderophore from *Vibrio vulnificus*. *Biometals* **7,** 109–116